Passive Electrical Measurements for Long-Term Performance Monitoring – 10034

Carlyle R. Miller, Ph.D.* and Mindy McCarthy*
* MSE Technology Applications, Inc., Butte, Montana 59701

ABSTRACT

MSE Technology Applications, Inc. (MSE) is developing a system for long-term field data acquisition and monitoring. The need for such a system is prevalent at numerous U.S. Department of Energy (DOE) sites undergoing contaminant remediation. Each site is unique so that no single system is universally applicable; however, there are several desirable characteristics (e.g., minimal maintenance requirements, ability to transmit and receive information remotely, adaptable to changing site conditions) for a monitoring system that generally apply to nearly any potential field site. MSE's prototype Meteor Burst Data Acquisition and Transmission System (MBDATS) is able to deliver these desirable characteristics and also has the added benefit of an integrated electrical data acquisition system for completing electrical resistivity, induced polarization (IP), and self-potential (SP) surveys. Electrical methods are useful for initial site characterization, contaminant plume delineation, time-lapse monitoring, leak detection, and many other environmental monitoring applications.

One possible long-term monitoring application of electrical methods is to monitor the performance of a permeable reactive barrier (PRB). Changes in the groundwater flow regime and the geochemistry of the subsurface are closely associated with the aging or degradation of PRBs. With appropriate data acquisition and analysis, electrical methods can be used to monitor and detect such changes over the lifetime of a PRB. The integration of electrical data into a site monitoring plan may reduce the need for monitoring wells, providing substantial cost savings over the lifetime of a remediation effort.

INTRODUCTION

The U.S. Department of Energy (DOE) faces a substantial challenge to remediate soils and groundwater at 60 contaminated sites in 22 states. Currently, there are over 300 remedies in place at these contaminated sites, and there is a need for state-of-the-art tools to monitor the performance of these remedies over the long term.[1]

MSE has been testing applications of the electrical self-potential (SP) method as a long-term performance monitoring tool. Electrical SPs are sensitive to subsurface processes and properties controlling groundwater flow and contaminant transport. Self-potential is a passive, distributed (bulk) measurement method requiring minimal equipment and infrastructure. Data acquisition using the SP measurement method is low in cost, and the SP data is compatible with the MSE Meteor Burst Data Acquisition and Transmission System (MBDATS), which provides site managers near real-time access to the data.

The SP method uses measurements of naturally occurring electrical potentials to infer information about subsurface properties and processes. The potentials that are measured result from a combination of electrical current sources related to pressure, chemical, and temperature gradients in the subsurface. Sill recognized that this multiplicity of sources could be considered either advantageous or nonadvantageous [1]. On the one hand, a number of different subsurface phenomena can be studied with the SP method; on the other hand, it may prove challenging to distinguish one source from another, leading to difficulties in interpreting SP data. Minsley remarked [2]:

[1] Dr. Vincent Adams, oral presentation at Oak Ridge SSAB, November 12, 2008.

> "The goal of a self-potential survey is to infer some properties about the source processes from the measured data. This is in contrast with other geophysical methods such as seismic, radar, or electrical resistivity tomography, which utilize known sources to actively probe structures in the subsurface. Self-potentials are therefore able to provide unique information about physical and chemical phenomena occurring in the earth that cannot be determined with other methods."

Previous Work

Past development of the SP method was motivated primarily by the mining industry in the search for sulfide ore deposits [3]; however, recent advancements in modeling and computing capabilities have led to the SP method being used more frequently in environmental applications. Research efforts over the past few years have demonstrated the utility of the SP method for mapping organic contaminant plumes [4,5], monitoring infiltration [6,7], monitoring changes in water level [8], mapping redox potentials [9], and monitoring pH and concentration fronts [10].

Present Work

MSE is actively researching applications of the SP method as a means for long-term monitoring of contaminated sites and ongoing remediation efforts at these sites. Specifically, the testing described herein focused on the use of SP data in monitoring permeable reactive barriers (PRBs). The utility of SP data in PRB monitoring is somewhat site specific; however, SP data is sensitive to a number of physical and chemical parameters that may change over the lifetime of a PRB and may even be useful for predicting PRB failure prior to its occurrence. Permeable reactive barriers are emplaced perpendicular to groundwater flow but are not designed to obstruct the movement of groundwater; rather, PRBs are designed so that groundwater is treated in situ as it flows through the barrier. As contaminants pass through the barrier, they react with the barrier materials in a manner that reduces the mobility or toxicity of the contaminants. For example, a barrier composed of zero-valent iron (ZVI) can be used to reduce hexavalent chromium [Cr(VI)] to trivalent chromium [Cr(III)], the latter being less mobile and less toxic than the former. Permeable reactive barriers have been successfully used for remediation of a number of contaminated DOE sites [11]. Current monitoring protocol for PRBs relies almost exclusively on monitoring wells drilled into and around a barrier.

METHODS

Testing methods to determine the feasibility of using electrical measurements for PRB monitoring included electrical SP, electrical resistivity and induced polarization (IP), water flow parameter measurements, and water quality parameter measurements. Each testing method is described briefly in this section.

Electrical Self-Potentials

Self-potentials are electrical potentials associated with passively sourced subsurface electrical currents. The magnitude of these electric potentials ranges from a few millivolts to tens and in some cases hundreds of millivolts over short distances (tens of meters or less). The electrical currents (fluxes) are due to some combination of forcing mechanisms (fields). The field-flux relationships can be summarized in the general form (Eq. 1):

$$q_i = \sum_j L_{ij} X_j \; ; \qquad \text{(Eq. 1)}$$

where q_i are the fluxes, X_j are the fields, and L_{ij} are coupling coefficients (physical properties of the material, generally tensor quantities) that provide a linear mapping between fields and fluxes. There exist several possibilities for coupled transport phenomena (field-flux relationships) in the subsurface (Table I).

For example, in Ohm's Law: $j = \sigma E$, electrical conduction current (j) is proportional to the electric field (E), in this case the coupling coefficient is the electrical conductivity (σ) of the medium through which the current propagates.

Table I. Possibilities for Coupled Transport Phenomena (from [2]).

		FORCES			
		Electric Gradient	Hydraulic Gradient	Chemical Gradient	Temperature Gradient
FLUXES	Electric	Ohm's Law	Electrokinetic Effect	Electrodiffusion	Seebeck Effect
	Fluid	Electro-Osmosis	Darcy's Law	Chemico-Osmosis	Thermo-Osmosis
	Solute	Electrophoresis	Ultrafiltration	Fick's Law	Soret Effect
	Heat	Peltier Effect	Thermal Filtration	Dufour Effect	Fourier's Law

Focusing on the top row of coupled transport relationships in Table I, it can be seen that the electrical current that gives rise to SPs is composed of some combination of conduction current, streaming current, diffusion current, and thermally forced current (Eq. 2).

$$j(x) = j_c(x) + j_k(x) + j_d(x) + j_t(x) \quad \text{(Eq. 2)}$$

The observed SP signal contains a superposition of effects from all of these current sources. In other words, the SP measurement does not discriminate the source of the electric potential. Additional information (from other geophysical methods, point measurements, groundwater sampling, etc.) is required to decouple the SP signal and separately analyze the various current forcing mechanisms.

Self-Potential Modeling

The SP data can be analyzed in its raw or filtered form; however, numerical modeling of the data provides for more rigorous analysis and interpretation of the data. A three-dimensional (3-D) numerical forward and inverse modeling routine was developed as part of this testing. The inputs to the modeling include the locations of the SP electrodes, the observed SP data, and the electrical resistivity structure of the medium (in this case the flow cell). The output of the modeling is a 3-D volumetric representation of electrical current sources and sinks. Thus, one can begin with SP data acquired on the surface (or from buried electrodes) and use it to infer the locations and magnitudes of electrical currents within the medium that give rise to this data. The modeling routine is implemented in MatLab® and is based on SP modeling work done by Minsley et al. [12]. Most of the details of the modeling are omitted here but can be found in the Minsley et al. [12] reference and references therein.

A requirement of the modeling is that resistivity values must be assigned throughout the model domain. If resistivity data is unavailable, these values can be estimated; however, errors and assumptions in the estimation will propagate through the modeling process, leading to errors and or bias in the solution. For this testing, resistivity data was acquired, thus the resistivity values used were a good estimate of the actual resistivity within the flow cell.

To construct a 3-D model of subsurface current sources, an iterative approach is used. The initial current source model is determined using a damped least square solution [13] that satisfies the data constraints (i.e., the model is expected to fit the data observations within some tolerance) while adhering to some additional constraints on how simple or complex the solution is expected to be. If the modeling grid is

not too coarse, the first iteration can be tuned to fit the data exactly; however, this is not always the ideal solution. Often, the initial solution will contain a great deal of structure in the vicinity of the electrode locations due to the higher data sensitivities in these regions. To construct more realistic models with structure away from the electrodes, further iterations are required. The iteratively reweighted least squares (IRLS) method [14] uses the initial damped least squares solution as a starting point then iteratively constructs new models that are increasingly more compact yet fit the data equally well.

Electrical Resistivity

An electrical resistivity measurement is made by injecting electrical current into the earth and measuring the resulting electrical potential field; this is usually performed using a four-electrode arrangement comprising two grounded electrical dipoles. Current is injected using one dipole, and a voltage is measured using the other dipole. In this manner, one can measure the volume-averaged resistivity (apparent resistivity) of the heterogeneous subsurface. By varying the electrode locations and spacing, lateral and depth variability of the apparent resistivity can be determined. Historically, apparent resistivities were interpreted directly; however, modern computing facilitates more rigorous two-dimensional (2-D) and 3-D numerical modeling of the data from which reconstruction of property distributions (resistivity/conductivity) is possible. Electrical resistivity data is sensitive to the electrical properties of the subsurface and is useful in imaging properties and processes associated with groundwater and unsaturated zone systems [15-18].

Induced Polarization

In the time-domain IP method, as in the electrical resistivity method, current is injected into the ground via an electric dipole. However, in IP work, the electrical current waveform has two off-cycles during each full period, and during the off-cycles, the voltage decay is measured within one or more time windows. The rate at which the voltage decays depends on the chargeability of the subsurface materials which, in turn, depends on the surface area, pore throat size, etc., of the investigated materials. Induced polarization data is sensitive to interfaces between regions of contrasting resistivity, such as the interface between fluid and host rock, and is especially sensitive to interfaces where there is a shift from ionic conduction to electronic conduction or vice-versa. Thus, IP is considered a very good method for the detection of disseminated metals. Slater and Binley [19] favor IP vs. other low-frequency electrical methods for in situ verification of PRB installations.

Water Flow and Quality Parameters

Water flow parameters measured during testing included flow rate and piezometric head. Flow rate through the test cell was regulated by a calibrated peristaltic pump so that only occasional calibration checks were necessary. These checks were accomplished using a stopwatch and graduated cylinder and if discrepancies in flow rate were found, the pump was recalibrated as necessary. Piezometric head was logged in two separate locations using combination pressure-temperature sensors with built-in data logging capabilities.

Water quality parameters measured for this testing included fluid conductivity, dissolved oxygen (DO) content, oxidation-reduction potential (ORP), temperature, and pH. Measurement instrumentation included a YSI 556 multiparameter probe and an Orion pH electrode. Instruments were calibrated prior to each use with standard solutions and the procedures outlined in the respective user's manuals for the equipment.

TESTING PREPARATION

Flow Cell

Testing was performed in a fiberglass tank designed to replicate groundwater flow in an unconfined aquifer (Fig. 1). The main compartment of the tank is approximately 2.06 meters (m) long, 1.22 m wide,

and 1.22 m deep. Within this compartment are nine polyvinyl chloride (PVC) wells (Fig. 1). The central well has an inside diameter (ID) of 52.5 millimeters (mm), and the remaining wells have an ID of 35.1 mm. The wells are screened to allow for water flow with a slot size of 0.2 mm. The screened interval extends from a point approximately 0.15 m above the bottom of the tank and continues to a point above the rim of the tank. The tank was filled to a depth of 0.86 m with 30-70 silica sand.

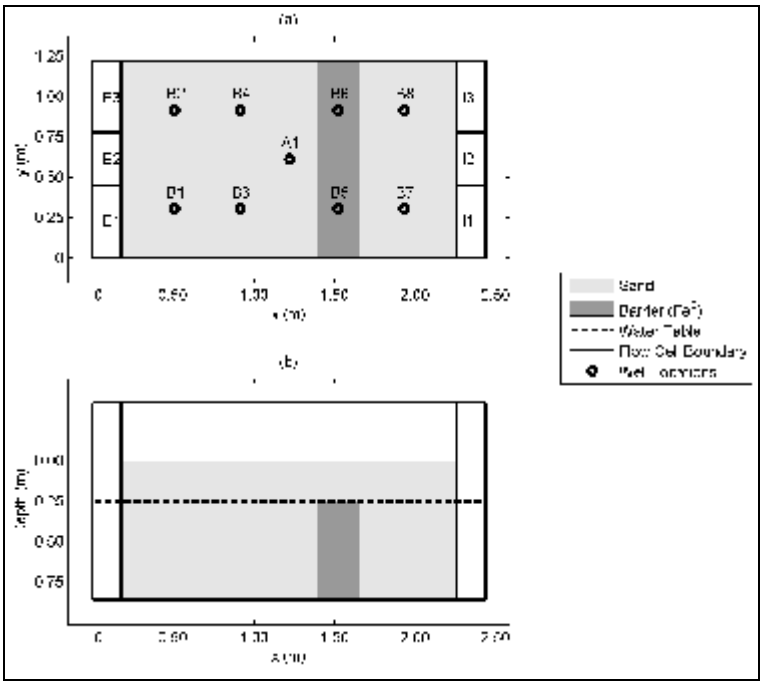

Fig.1. Scale drawings of the flow cell showing the locations of the wells, sand matrix, water table, and the PRB: water flow direction is from right to left. (a) top view; (b) side view.

Installation of the Zero-Valent Iron Barrier

Fine iron aggregate was mixed with 30-70 silica sand in a ratio of 33% iron aggregate to 67% sand (by volume) to form the ZVI barrier material. A trench box was used to ensure that the emplaced ZVI barrier was 0.25 m long, 1.22 m wide, and 0.61 m deep. The ZVI barrier (Fig. 1) was installed so that it completely encompassed two of the monitoring wells (wells B5 and B6). The bottom of the ZVI barrier is coincident with the bottom of the flow cell. After the ZVI barrier was emplaced, the trench box was removed from the tank, and the sand was smoothed and leveled. Some additional sand was added to the tank to fill in low areas.

Water Flow System

The water source used for the testing was the plant supply water in Building 50 of the MSE Test Facility in Butte, Montana (Table II). This water was filtered (2 stages, 3 micron then 1 micron) in an attempt to remove iron particulate. After exiting the filter, the water was routed into an approximately 757-liter (L) polyethylene tank. An aerator pump was continuously operated (from February 16, 2009, through the end of testing on April 27, 2009) in the poly tank to increase the DO content of the water prior to introducing it into the flow cell. The purpose of the increased oxygen level in the influent water was to enhance the degradation of the reactive ZVI barrier. A peristaltic pump was used to pump water from the poly tank into the influent reservoir of the flow cell at a constant rate of 150 milliliters (mL) per minute. On the effluent end of the flow cell, a standpipe outlet was used to maintain a constant head of approximately 0.61 m measured from the bottom of the tank.

Table II. Chemistry of the Water Used During Testing.

Parameters	Conductivity	DO	ORP	pH	TDS
	175 (μS/cm)[a]	5 (mg/L)[b]	214.4 (mV)[c]	6.97 (su)[d]	107 (mg/L)
Cations (mg/L)	Calcium	Magnesium	Potassium	Sodium	
	17.1	6.72	2.36	4.14	
Anions (mg/L)	Alkalinity	Chloride	Nitrate	Sulfate	
	51.26	3.98	0.05	21.7	
Other (μg/L)[e]	Iron (total)				
	800				

[a] μS/cm = microSiemens per centimeter.
[b] mg/L = milligrams per liter.
[c] mV = millivolt.
[d] su = standard unit.
[e] μg/L = micrograms per liter.

Instrumentation

A total of 29 nonpolarizable lead-lead chloride (Pb-PbCl) electrodes were installed in the tank for measuring the SP field; 20 of these electrodes were located at the surface on a regular, orthogonal grid, and 8 electrodes were installed at depth (4 at 0.41-m depth, 4 at 0.76-m depth) within the ZVI barrier during emplacement. The final electrode was used as a common ground reference for the SP measurements. The reference electrode was initially installed at the surface to facilitate SP data acquisition during tank filling; however, later the reference electrode was moved into the influent reservoir. The influent reservoir, being located upgradient of the barrier, was minimally influenced by changes within the barrier and was thus a more appropriate long-term location for the reference electrode. In a field application, the reference electrode should be placed some distance away from the potential electrodes, ideally in a location that will not be affected by the geochemistry of the barrier (e.g., upgradient of the barrier) and away from sources of electrical interference. The reference electrode should also be buried to a depth where diurnal temperature variations will not influence the electrode. Due to the confined boundaries of the flow cell, removal of the reference electrode from the source region during this testing was not possible. To improve electrical contact with the sand and to prevent drying of the electrodes, the electrodes were installed into a ball of saturated bentonite that was then buried in the sand.

Pressure/temperature sensors were installed in Well A1 and in the effluent reservoir compartment. Six ORP electrodes were installed in various locations, including two electrodes within the barrier itself. The data from the SP and ORP electrodes were monitored using multichannel data loggers; the data from the pressure/temperature sensors were logged internally by the sensors themselves.

Testing Conditions

For the majority of the testing duration, groundwater flow through the test cell was maintained at a constant rate of 150 mL/minute, and the saturated zone was maintained at an average thickness of 0.61 m (being slightly thicker on the influent end of the flow cell and slightly thinner on the effluent end).

DATA ACQUISITION

Data acquisition began soon after the ZVI barrier was emplaced in the tank and continued for several weeks. Table III provides details on sampling rates and equipment used for the various data acquisition.

Table III. Data Sampling Rates and Equipment.

Data Description	Sampling Rate	Equipment Required
SP	Every 15 minutes	Pb-PbCl electrodes, CR23X datalogger
Electrical resistivity and IP	Occasional	Syscal R2 resistivity/IP system, Pb-PbCl electrodes, copper electrodes
pH and temperature	2-3 times weekly	Orion pH electrode
pH, ORP, SC[a], DO, temperature	2-3 times weekly	YSI 556 multiparameter probe
Pressure and temperature	Every 15 minutes	In situ level troll
Pressure and temperature	Every 15 minutes	Instrumentation Northwest PT2X
ORP	Every 15 minutes	Cole-Parmer ORP electrodes, CR23X datalogger

[a] SC = specific conductance.

Electrical Resistivity and Induced Polarization

The electrical resistivity and IP data were acquired using a dipole-dipole electrode configuration. Copper stakes were used for current injection, and nonpolarizable Pb-PbCl electrodes were used for voltage measurements. Contact resistance for the electrodes was variable but was typically ranged from 4 to 8 kilo-ohms (kΩ). A Syscal R2 resistivity/IP meter was used to acquire the data. The source current frequency was 0.5 hertz (period = 2 seconds), and the data were averaged for a minimum of six measurements to determine noise levels in the data.

RESULTS AND INTERPRETATION

An important application of PRB monitoring is to detect degradation of a barrier over time in an attempt to predict failure of a barrier before its occurrence. However, after initial barrier installation there is often a "ripening" time while the geochemistry of the barrier achieves equilibrium with the surrounding medium. Due to the relatively short duration of this test (many barriers are designed to operate for decades vs. the 10-week monitoring period for this test), many of the geochemical changes noted in this section may indicate barrier ripening rather than degradation.

Water Level and Temperature Monitoring

Changes in water level and water temperature can strongly influence SP measurements. To the extent possible, water level and temperature were regulated and monitored. The water table was maintained at approximately 0.61 m for the duration of testing. Water temperature varied smoothly between 17 °C and 23 °C throughout testing. The temperature changes resulted from variable residence times for the water in the poly tank prior to pumping it into the flow cell.

Water Quality Monitoring

Although the electrokinetic (streaming current) is typically the strongest contributor to the SP signal, water quality parameters can also be shown to affect the data. Frequent water quality parameter sampling was performed throughout the duration of the testing to ensure variations in these parameters were quantified and understood. Fluid pH, ORP, and DO all responded as expected to the ripening of the PRB. In the region located just downgradient from the PRB, the pH rose from approximately 7.4 to 9.0, ORP fell from 100 mV to –240 mV, and DO fell from 6 mg/L to 1 mg/L. Parameters in the region upgradient of the PRB remained near their initial magnitudes throughout testing.

Hydrochloric acid (HCl) had been injected into specific regions of the flow cell as part of a previous test. Via the pH monitoring, it was discovered that there were some residual low pH regions left in the flow

cell from this test, even after flushing the flow cell for several pore volumes. The implications of this localized region of residual low pH on the SP measurements will be discussed in a later section.

Self-Potential Modeling

Self-potential modeling was completed using the surface SP data from several different times throughout the testing. The reason that only the surface data, and not the buried data, was inverted is that the solutions including the buried data tended to have a bias toward current sources within the ZVI barrier (where the buried electrodes are located). If these current sources actually exist, they should be able to be resolved using the surface data (albeit with diminished resolution) without the added complication of possible sensitivity bias. The resistivity values used in the modeling were extracted from the 3-D resistivity model based on data acquired on February 4-5, 2009, under steady-state flow conditions. The resistivity of the test cell did not change significantly throughout the testing (except when water levels changed significantly), thus this particular resistivity model was used in the modeling of all of the SP data, including the SP data acquired during tank filling, for which no resistivity data was available.

Time-Slice Self-Potential Modeling

Modeling of the SP data (mV) from a specific time allows construction of a "snapshot" of the current sources (μA) in the tank at that particular time. Intuition suggests that the current source distribution would be different during the tank filling than it would be later during steady-state flow. As can be seen in Fig. 2, time-slice models confirm this assumption. The top six plots of Fig. 2 show depth slices of the source current distribution on January 26, 2009, at 9 a.m. At this time, the flow cell was being filled with water and was approximately three-fourths full. In the shallowest depth section, there are some strong negative current sources (current sinks). This shallow structure likely results from the preferential fitting of structure near the electrode locations in order to better fit the data and is thus not considered as true structure. In the deeper sections, there are strong current sources associated with the ZVI barrier and strong current sinks downgradient of the barrier. This suggests that currents are being generated by water flowing through the barrier via either electokinetic or electrochemical effects (or a combination). The bottom six plots in Fig. 2 show the source current distribution on February 19, 2009, at 6 a.m. during steady flow through the tank. In this case, the strongest anomalies are along the north (top as plotted) and south (bottom as plotted) edges of the flow cell. These elongated source current anomalies are interpreted as resulting from electrochemical gradients caused by the lower pH in the northern half vs. the southern half of the flow cell.

Time-Lapse Self-Potential Modeling

The time-lapse SP modeling is similar to the time-slice SP modeling except that difference data, rather than raw data, is inverted. Differences in the SP data can arise from either changes in the electrical current distribution within the medium or from noise. The primary noise source in long-term SP measurements is electrode drift over time; this electrode drift can occur at the reference electrode or at any of the measurement electrodes. If the drift occurs only at the reference electrode, this will result in a shift of the potential measured by all of the electrodes and will not significantly affect the modeling results. However, if one of the measurement electrodes drifts with respect to the other electrodes, this will potentially result in extraneous model structure necessary to fit this noise. There is no simple method to distinguish actual signal from noise, but knowing where changes are occurring in the medium (from other data sources) can aid in the interpretation of the final model. For example, in the flow cell, it would be expected that changes in pH and ORP would cause changes in the electrical current distribution. By measuring the pH and ORP, one can anticipate which regions of the flow cell will give rise to changes in the measured SP data and thus possibly distinguish signal from noise in this manner.

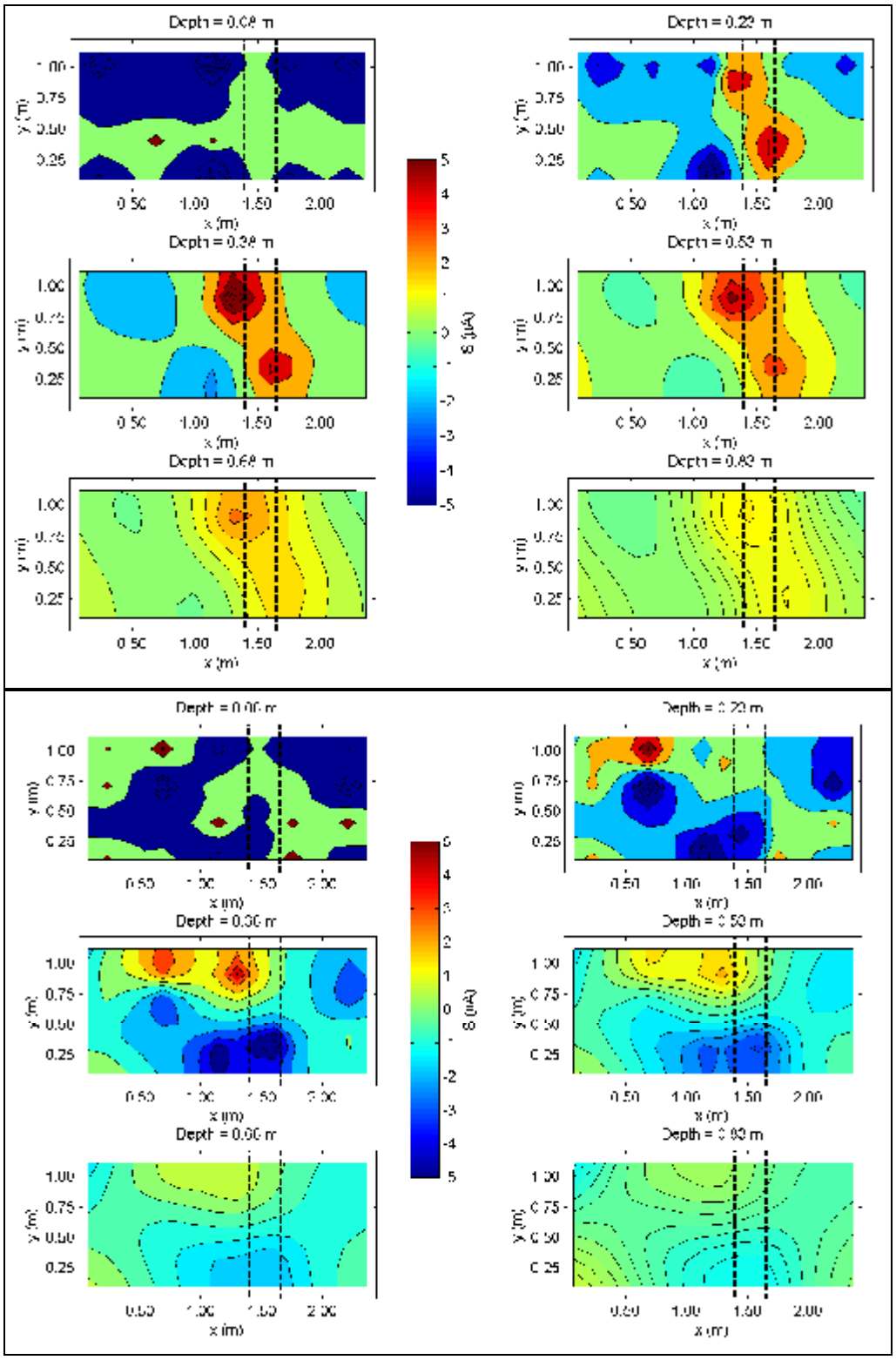

Fig. 2. The top six plots show depth slices from the 3-D model of electrical current sources on January 26, 2009, at 9 a.m. The bottom six plots show depth slices from the 3-D model of electrical current sources on February 19, 2009, at 6 a.m. The dashed black lines included on all plots indicate the lateral extent of the barrier. Water flow direction is from left to right.

The time-lapse difference data was constructed by subtracting the data at time = t_0 from the data at time = $t_0 + \Delta t$ (where Δt is positive), thus a negative value in the model represents a decrease in the magnitude of current sources, and a positive value in the model represents an increase in the magnitude of current sources. The top six plots in Fig. 3 show depth slices from a time-lapse difference model of electrical current sources for a 3-hour time window on January 26, 2009. In this set of plots, the strongest anomalies are along the edges of the ZVI barrier and along the downgradient edge of the flow cell where the water departs the flow cell and enters the effluent reservoir. These changes in the source current distribution most likely arise from electokinetic sources caused by changes in the vadose zone thickness within the tank as the water level increases. There may also be some electrochemical source changes; however, these are difficult to decouple from gradient changes when both processes are occurring simultaneously. The bottom six plots in Fig. 3 show depth slices from a time-lapse difference model of electrical current sources for an 11-day time period between February 9-19, 2009. The flow conditions during this time were long-term sustained steady flow through the test cell. The strongest anomalies in this series of plots are clearly associated with the ZVI barrier and with the region of lower pH in the northwest corner (top left as plotted) of the test cell. Because flow rate and water table height were essentially unchanged during this time period, these anomalies are interpreted as resulting entirely from electrochemical changes occurring in the tank. Within the barrier, oxygenated water is oxidizing the iron while the low pH region is being continuously flushed with higher pH water that is exiting the barrier, slowly equilibrating the pH in this region with the remainder of the flow cell.

Resistivity and Induced Polarization Measurements

Electrical resistivity and IP data were acquired several times over the duration of the testing. Modeling of the electrical resistivity and IP data was completed using RES2DINV™ and RES3DINV™ software by GeoTomo [20]. Self-potential data acquisition was not suspended during resistivity and IP measurements. It was noted that the SP measurements exhibited strong interference during the resistivity and IP acquisition; however, the effect is temporary. On completion of resistivity and IP acquisition, the SP measurements stabilized to levels observed prior to the resistivity and IP acquisition within approximately 4 to 5 hours. Both 2-D and 3-D resistivity and IP data were acquired; however, due to space limitations, analysis herein is limited to some of the 2-D time-lapse resistivity and IP imaging.

Two-Dimensional Resistivity and Induced Polarization Results

Time-lapse resistivity and IP acquisition are useful for imaging the changes in subsurface electrical resistivity and chargeability structure. In this case, a change was imposed in the flow cell by lowering the water table by approximately 0.3 m. After allowing the system to stabilize for several hours, time-lapse resistivity and IP data were acquired. The time-lapse data was acquired only along Line 2 because data along this line appeared less prone to edge effects from the flow cell walls. All of the time-lapse difference models were constructed by subtracting the time = t_0 data from the time = $t_0 + \Delta t$ data (where Δt is always positive). The top two plots in Fig. 4 show two resistivity models (one before lowering the water table and one after) from Line 2 modeled simultaneously using a smoothness constraint. The constraint is applied to the difference in the logarithms of each model, thus the percent difference between the models was calculated using the logarithms of the models (third plot in Fig. 4). The largest differences between the two models are located in close proximity to the ZVI barrier. This localized increase in resistivity most likely results from the faster (and more complete) desaturation of the barrier materials due to their slightly larger average grain size vs. the background material within the flow cell.

In the time-lapse IP results (bottom three plots of Fig. 4), the largest change in chargeability was a marked decrease in the vicinity of the ZVI barrier. Presumably, this decrease is also related to the dewatering of the flow cell. Prior to lowering the water table, electric currents traversing the barrier shifted between ionic and electronic conduction. With the water table lowered, the ionic conduction mechanism was weaker; therefore, the chargeability contrast between the barrier and the background materials in the flow cell became less pronounced.

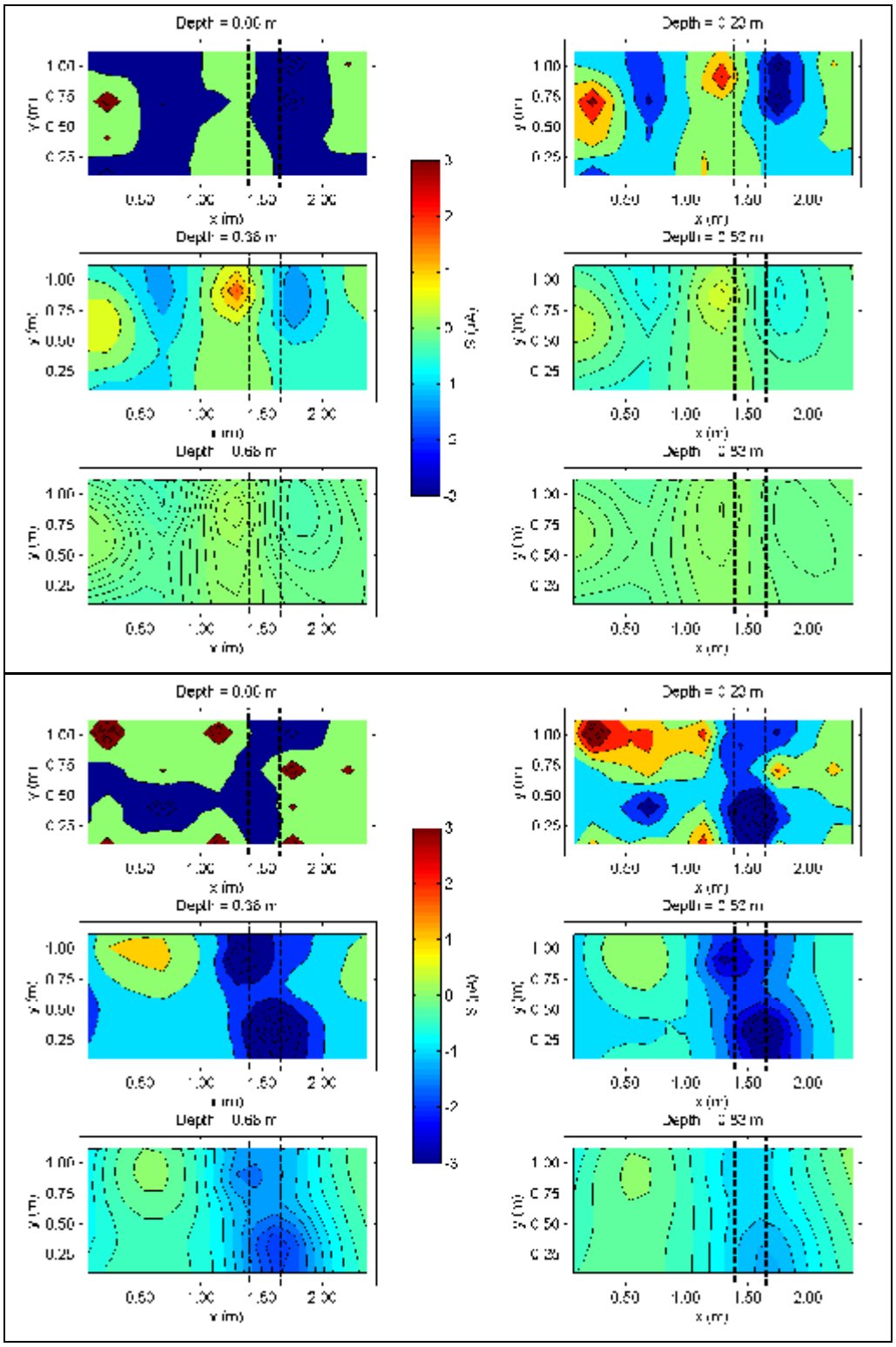

Fig. 3. The top six plots are depth slices from the 3-D difference model of electrical current sources on January 26, 2009, between 6 a.m. and 9 a.m. The bottom six plots are depth slices from the 3-D difference model of electrical current sources from February 9-19, 2009. The dashed black lines included on all plots indicate the lateral extents of the barrier. Water flow direction is from left to right.

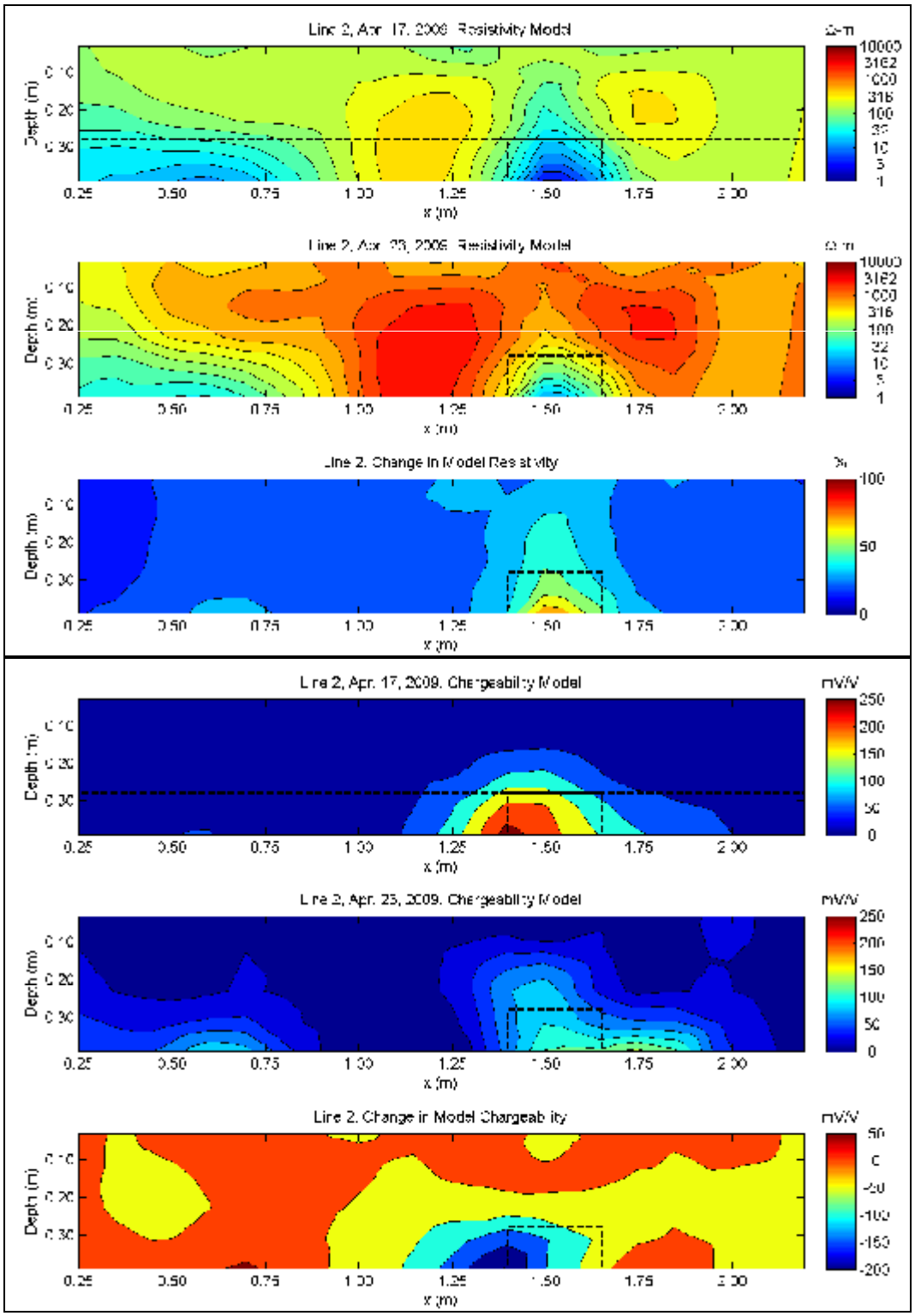

Fig. 4. The top three plots are images from 2-D time-lapse resistivity modeling before and after lowering the water level in the flow cell. The bottom three plots are images from 2-D time-lapse IP modeling before and after lowering the water level. For all plots, dashed lines indicate the approximate location of the ZVI barrier and, as applicable, the water table.

SUMMARY AND CONCLUSIONS

Although analysis of self-potential data can be complicated by electrode drift and external interferences, the SP measurements are simple to acquire and contain a wealth of information about subsurface properties and processes. Long-term monitoring using SP measurements can be difficult because of noise introduced by electrode drift over time; even relatively stable electrodes can experience drift on the order of several millivolts over the course of a year. This complicates the data analysis because there is no simple way to distinguish this electrode noise from the desired signal in the measurements. The best solution is to acquire supplementary data (e.g. water flow and quality parameters) along with the SP data so that the SP measurements can be analyzed and interpreted within the context of these other measurements.

For this test, SP data was acquired within a flow cell containing a ZVI barrier. To simulate the long-term aging of a ZVI barrier over time, oxygen-enriched water was flowed through the barrier at a nearly constant rate for several weeks. The rate of oxygen consumption by the barrier was approximately 5 mg oxygen per liter of water, which had the effect of slowly oxidizing the iron in the barrier as the test progressed. This aging of the barrier was imaged using time-lapse difference modeling of the SP. There was also a region of low pH in the test cell, resulting from residual HCl left in the cell after a previous test. The time-lapse SP analysis provided images of the electrochemical changes in this region as the high pH water exiting the barrier slowly mixed with the lower pH fluid and soils in this region. Self-potential data acquired during the initial saturation of the tank was used to construct images of the electrical current source distribution during this time. These images indicated lateral contrasts in the electrokinetic coupling coefficient along each edge of the barrier, which was due to both the different particle size range and the different composition of the barrier materials vs. the homogenous sand on either side of the barrier.

Quantitative analysis of the SP data was accomplished via 3-D numerical modeling of the SP measurements. An important aspect of this modeling was that it required an estimate of the electrical resistivity structure of the test cell in order to accurately reconstruct the source current density. Electrical resistivity data was acquired in the test cell on several occasions, and the best 3-D model of electrical resistivity was then incorporated into the SP modeling. The modeling input can be either the SP data or SP difference data; the difference data modeling proved especially useful for imaging changes in SP source mechanisms within the flow cell. Self-potential data was acquired from electrodes installed within the barrier, but it was determined that incorporating this data into the modeling might introduce unnecessary bias into the final results. Of note is that the modeling still clearly imaged the barrier despite the fact that only surface SP measurements were used. This suggests that this method could be useful for monitoring of legacy barrier installations where it may be too difficult or costly to install electrodes within the barrier itself. Installation of electrodes at the surface is relatively simple, minimally invasive, and inexpensive, and results from this test indicate that surface electrodes provide ample information about deeper processes within the region surrounding the barrier.

Induced polarization imaging was also useful for delineating the extents of the barrier. Induced polarization data is easily acquired during resistivity data acquisition, having identical equipment and personnel requirements as for resistivity acquisition. For this testing, no time-lapse IP measurements were analyzed; however, such analysis could potentially further aid in the interpretation of the SP difference measurements.

Considering the results of this testing, long-term monitoring of PRBs using electrical methods could be accomplished using the following approach:

- during construction of the barrier, install electrodes within and surrounding the barrier at various depths and install a regular grid of surface electrodes;

- after the barrier installation is complete, acquire baseline electrical resistivity and IP data;
- monitor the SP regularly and occasionally complete time-lapse measurements of the electrical resistivity and IP; and
- occasionally monitor parameters such as ORP and pH for supporting information.

This approach would provide site managers with baseline images of the geoelectrical structure of the site and the ability to image changes in these conditions as the barrier ages and degrades. Ideally, this approach would provide adequate early warning of imminent barrier failure.

It should be reiterated that the results discussed in this report apply to this small-scale domain where the vertical distance between the barrier and the surface was minimal; likewise, the distance between the SP electrodes was much less than would be typically used in a field setting. The testing was conducted in laboratory conditions where there were no significant changes in ambient temperature or moisture content of the unsaturated zone and within a nonconductive tank that limited the influence of galvanic electrical interferences (the tank was not shielded from inductive interference). Field implementation of electrical monitoring of PRBs merits further investigation and research to determine the capabilities and limitations of the approach.

ACKNOWLEDGEMENTS

This work was conducted through the DOE Environmental Management Consolidated Business Center at the Western Environmental Technology Office under DOE Contract Number DE-AC09-96EW96405. Mr. Sean Colligan (MSE) and Ms. Emma Hyde (Montana Tech of the University of Montana) provided valuable assistance with data acquisition.

REFERENCES

1. W.R. Sill, "Self-Potential Modeling from Primary Flows," *Geophysics*, *48*, 76-86 (1983).
2. B.J. Minsley, *Modeling and Inversion of Self-Potential Data*, Ph.D. Thesis, Massachusetts Institute of Technology (2007).
3. M. Sato and H.M. Mooney, "The Electrochemical Mechanism of Sulfide Self-Potentials," *Geophysics*, *25*, 226-249 (1960).
4. T. Arora, A. Revil, N. Linde, and J. Castermant, "Nonintrusive Determination of the Redox Potential of Contaminant Plumes using the Self-Potential Method," *Contaminant Hydrology*, *92*, 274-292 (2007).
5. N. Linde and A. Revil, "Inverting Residual Self-Potential Data for Redox Potentials of Contaminant Plumes," *Geophysical Research Letters*, *34*, L14302 (2007).
6. B. Suski, A. Revil, K. Titov, P. Konosavsky, M. Voltz, C. Dagès, and O. Huttel, "Monitoring of an Infiltration Experiment using the Self-Potential Method," *Water Resources Research*, *42*, W08418 (2006).
7. A. Jardani, A. Revil, F. Santos, C. Fauchard, and J.P., Dupont, "Detection of Preferential Infiltration Pathways in Sinkholes using Joint Inversion of Self-Potential and EM-34 Conductivity Data," *Geophysical Prospecting*, *55*, 1-11 (2007).
8. N. Linde, A. Revil, A. Bolève, C. Dagès, J. Castermant, B. Suski, and M. Voltz, "Estimation of the Water Table throughout a Catchment using Self-Potential and Piezometric Data in a Bayesian Framework," *Journal of Hydrology*, *334*, 88-98 (2007).
9. J. Castermant, C.A. Mendonça, A. Revil, F. Trolard, G. Bourrié, and N. Linde, "Redox Potential Distribution Inferred from Self-Potential Measurements during the Corrosion of a Burden Metallic Body," *Geophysical Prospecting*, *56*, 269-282 (2008).

10. A. Maineult, Y. Bernabé, and P. Ackerer, "Detection of Advected Concentration and pH Fronts from Self-Potential Measurements," *J. Geophys. Res.*, *110*, B11205, doi:10.1029/2005JB003824 (2005).
11. DOE, *Groundwater Contamination and Treatment at Department of Energy Sites* (August 2008).
12. B.J. Minsley, J. Sogade, and F.D. Morgan, "Three-Dimensional Source Inversion of Self-Potential Data," *J. Geophys. Res.*, *112* (B02202) (2007).
13. A.N. Tikhonov and V.A. Arsenin, *Solutions of Ill-Posed Problems,* 258 pp., Winston & Sons, Washington (1977).
14. J.A. Scales and A. Gersztenkorn, "Robust Methods in Inverse Theory," *Inverse Problems*, *4*, 1071-1091 (1988).
15. L.D. Slater, A. Binley, and D. Brown, "Electrical Imaging of Fractures using Groundwater Salinity Change," *Ground Water*, *35*, 436–442 (1997).
16. Q.Y. Zhou, J. Shimada, and A. Sato, "Three-Dimensional Spatial and Temporal Monitoring of Soil Water Content using Electrical Resistivity Tomography," *Water Resources Research*, *37*, 273–286 (2001).
17. A. Binley, P. Winship, L.J. West, M. Pokar, and R. Middleton, "Seasonal Variation of Moisture Content in Unsaturated Sandstone Inferred from Borehole Radar and Resistivity Profiles," *Journal of Hydrology*, *267*, 160–172 (2002).
18. G.A. Oldenborger, M. Knoll, P. Routh, and D. LaBrecque, "Time-Lapse ERT Monitoring of an Injection/Withdrawal Experiment in a Shallow Unconfined Aquifer," *Geophysics*, *72*, F177–F187 (2007).
19. L.D. Slater and A. Binley, "Synthetic and Field-Based Electrical Imaging of a Zerovalent Iron Barrier: Implications for Monitoring Long-Term Barrier Performance," *Geophysics*, *71*, B129 (2006).
20. M.H. Loke and R.D. Barker, "Rapid Least-Squares Inversion of Apparent Resistivity Pseudosections by a Quasi-Newton Method," *Geophysical Prospecting*, *44*, No. 1, 131-152 (2006).